Published in final edited form as:
Neuron. 2008 October 23; 60(2): 343–352. doi:10.1016/j.neuron.2008.10.002.

Frequency-independent synaptic transmission supports a linear vestibular behavior

Martha W. Bagnall[1,2], **Lauren E. McElvain**[1,2], **Michael Faulstich**[2], and **Sascha du Lac**
[1]Neurosciences Graduate Program, University of California San Diego

[2]Salk Institute for Biological Studies, La Jolla CA

[3]Howard Hughes Medical Institute

Summary

The vestibular system is responsible for transforming head motion into precise eye, head, and body movements that rapidly stabilize gaze and posture. How do central excitatory synapses mediate behavioral outputs accurately matched to sensory inputs over a wide dynamic range? Here we demonstrate that vestibular afferent synapses *in vitro* express frequency-independent transmission that spans their *in vivo* dynamic range (5 – 150 spikes/s). As a result, the synaptic charge transfer per unit time is linearly related to vestibular afferent activity in both projection and intrinsic neurons of the vestibular nuclei. Neither postsynaptic glutamate receptor desensitization nor saturation affect the relative amplitude or frequency-independence of steady-state transmission. Finally, we show that vestibular nucleus neurons can transduce synaptic inputs into linear changes in firing rate output, without relying on one-to-one calyceal transmission. These data provide a physiological basis for the remarkable linearity of vestibular reflexes.

Introduction

The nervous system serves to transform sensory inputs into motor outputs via cellular and synaptic processes that are specialized for the behaviors they support. In this study, we examine the transformation from presynaptic to postsynaptic firing rate in the well-defined brainstem circuit of the vestibular system to identify the physiological underpinnings of a fast, linear behavior.

Head movements trigger vestibular reflexes that produce rapid and precise compensatory movements of the eyes, head, and body. During the vestibulo-ocular reflex (VOR), the eyes are directed contraversive to head motion in order to maintain a stable retinal image. The VOR exhibits two remarkable characteristics: first, the latency from onset of head motion to onset of eye movement is < 10 ms (Huterer and Cullen, 2002; Minor et al., 1999); and second, eye velocity accurately compensates for head velocity over a broad dynamic range in a variety of species, including goldfish, frogs, rodents, cats, and primates (Faulstich et al., 2004; Furman et al., 1982; Pastor et al., 1992; Pulaski et al., 1981; Robinson, 1976; Straka and Dieringer, 2004).

Correspondence should be addressed to Dr. Sascha du Lac (sascha@salk.edu).

These twin demands of speed and accuracy must be met by the supporting neuronal circuitry. The VOR relies on a trisynaptic pathway: information about head movement originates in the inner ear and is carried via vestibular nerve afferents to the brainstem vestibular nuclei; from there it travels to oculomotor nuclei (Fig. 1A). The brevity of this circuit keeps reflex times short. What qualities of the circuit ensure that eye velocity is precisely matched to head velocity over a wide dynamic range?

Vestibular afferents code primarily for head velocity (reviewed in Highstein et al., 2005), as do their postsynaptic targets, vestibular nucleus neurons (Beraneck and Cullen, 2007; Lisberger and Miles, 1980; Scudder and Fuchs, 1992). Given that the VOR operates accurately across a wide range of head velocities, transmission at the excitatory synapse from vestibular afferents onto vestibular nucleus neurons would be expected to be linear. However, transmission at most glutamatergic synapses is nonlinear: both the probability of transmitter release and the efficacy of postsynaptic response to that transmitter depend heavily on the recent history of the synapse (Zucker and Regehr, 2002). If the vestibular afferent synapse were to operate in this way, its ability to transmit precise signals about head velocity could be compromised.

We sought to determine whether synaptic transmission at the vestibular afferent synapse could succeed in linear information transfer. In this study, we record in voltage and current clamp from neurons in the vestibular nucleus while stimulating vestibular afferents in mouse brainstem slices. The results define the synaptic properties that produce a linear transformation from pre- to post-synaptic firing rates.

Results

The performance of the VOR was assessed by rotating awake mice back and forth on a turntable in the dark while a video camera captured their eye movements. Eye motion was similar in amplitude and opposite in direction to head motion, as evident in sinusoidal plots of head and eye velocity (Fig. 1B). Remarkably, eye velocity was linearly matched to head velocity over a 40-fold range of peak head velocities, from 4 to 157 °/s (Fig. 1C). Across all head velocities tested, the VOR successfully compensated for 80% of head motion (in the light, visual reflexes compensate for the remainder (Faulstich et al., 2004)). The mouse VOR is therefore linear over a wide dynamic range of head motion.

The brainstem circuit for the VOR is outlined in Fig. 1A. Vestibular information about rotational head velocity, derived from fluid movement in the semicircular canals, is carried via fibers of the VIIIth nerve to neurons in the vestibular nuclei. The medial vestibular nuclei (MVN), which process head motion in the horizontal plane, control the muscles for horizontal eye movement via projections to the oculomotor and abducens nuclei. Information about head velocity must be transformed into matched oculomotor responses through this circuit. How can head velocity be accurately converted into eye velocity across glutamatergic synapses, which are typically thought of as nonlinear elements (Abbott and Regehr, 2004)?

To address this question, we electrically stimulated vestibular afferents while recording from MVN neurons in slice preparation of the brainstem. Whole-cell patch clamp recordings were targeted to fluorescently labeled neurons in two transgenic mouse lines that label complementary neuronal distributions in the MVN: the YFP-16 line (Feng et al., 2000), which labels glycinergic and glutamatergic premotor projection neurons; and the GIN line (Oliva et al., 2000), which highlights a subset of local GABAergic neurons (Bagnall et al., 2007; Epema et al., 1988; Holstein, 2000; see also Experimental Procedures).

Stimulation of the vestibular nerve elicited synaptic currents in the majority of vestibular nucleus neurons, consistent with data suggesting that the vestibular nerve contacts most MVN neurons (Babalian et al., 1997; Goldberg and Fernandez, 1971; Lewis et al., 1989; Straka and

Dieringer, 1996). Increases in stimulation intensity led to increases in excitatory postsynaptic current (EPSC) amplitude, indicating that each neuron receives input from multiple vestibular afferent fibers (Fig. 2A). The maximal synaptic currents elicited in YFP-16 neurons ranged as high as 6 nA, while those in GIN neurons were typically less than 1 nA (Fig. 2B; $p < 0.0001$, Wilcoxon unpaired test). In both YFP-16 and GIN neurons, EPSCs exhibited rapid rise and fall kinetics (Fig. 2C, 2D). These data demonstrate that MVN neurons receive multiple fast synaptic inputs, with a larger maximum conductance in premotor than in local-projecting neurons, consistent with anatomical data (Huwe and Peterson, 1995; Sato and Sasaki, 1993).

In vivo, mouse vestibular afferents fire at ~30–70 spikes/s in the absence of head motion, and modulate above and below those firing rates during head motion (Lasker et al., 2008; Yang and Hullar, 2007). To evaluate the short-term dynamics of the synaptic response to repetitive activity, we stimulated presynaptic afferents with trains of 20 pulses at frequencies from 0.1 to 200 Hz. The paired-pulse ratio, measured as the ratio of the amplitude of the second EPSC to the first (Fig. 2E), was remarkably stable across these frequencies in both YFP-16 and GIN neurons. At the longest interval (10 s), no facilitation or depression was observed in either population; at intervals from 5 ms to 1 s, the paired-pulse ratio was ~0.85 in both types of neurons (Fig. 2F). This represents an unusual history-independent response, in contrast to the frequency-dependent transmission at many other types of synapses.

Over the course of 20-stimulus trains, EPSC amplitudes depressed during the first 5–10 stimuli and then reached a plateau of about 60% of their initial value for the remainder of the train (Fig. 3A, EPSCs recorded in a YFP-16 neuron during vestibular nerve stimulation at 20 and 100 Hz; Fig. 3B, the same for a GIN neuron). The number of stimuli, rather than the time course of their delivery, defined the rate of depression, as can be seen in plots of normalized EPSC amplitude relative to stimulus number (Fig. 3C). The absolute level of steady-state depression varied among neurons from 25–85%, but within any given neuron was constant across a wide range of stimulus frequencies (Fig. 3D). Therefore, in the steady state, EPSC amplitude is independent of afferent activity rates.

Given that the vestibular nerve fires action potentials at rates linearly related to head velocity (Highstein et al., 2005), the synaptic charge transfer over a given unit of time should be linearly related to the head motion signal, i.e. the presynaptic firing rate. A recent study on synapses from vestibular nucleus neurons onto cerebellar granule cells in anesthetized mice found a linear relationship between head velocity and charge transfer, over a range of EPSC frequencies from ~15–45 Hz (Arenz et al., 2008). To calculate charge transfer at the vestibular afferent synapse, EPSCs evoked during the plateau phase (pulses 11–20) were averaged, integrated and normalized to the integral of the first EPSC in the train. The resulting value for each stimulus was multiplied by the stimulus rate to obtain the total charge transfer during 1 s of steady-state activity. As shown in Fig. 3E, a linear relationship between the rate of stimulation and the total synaptic charge transfer per unit time was evident in both YFP-16 and GIN neurons, for frequencies ranging from 5 to 100 Hz (Fig. 3E).

Frequency-independent synaptic transmission must derive from one of two possibilities: either presynaptic release probabilities and postsynaptic glutamate sensitivity are constant across the relevant frequency domain; or nonlinearities of release are perfectly masked by corresponding nonlinearities of glutamate sensitivity. We tested in turn the two primary candidates for postsynaptic nonlinearities on this timescale, AMPA receptor desensitization and saturation (von Gersdorff and Borst, 2002).

At the homologous synapse in the auditory system, the endbulb of Held, postsynaptic AMPA receptor desensitization is responsible for some of the observed paired-pulse depression (Isaacson and Walmsley, 1996; Trussell et al., 1993; Yang and Xu-Friedman, 2008).

Desensitization might conceal an increase in vesicular release from vestibular afferents at higher rates of presynaptic activity (Wong et al., 2003). We tested this possibility by applying the desensitization antagonist cyclothiazide (100 μM) while recording EPSCs in the vestibular nuclei (Fig. 4A). Both decay times and peak amplitudes of synaptic currents were significantly increased by cyclothiazide (n = 6: decay time, mean 84 ± 27% increase; peak amplitude, 39 ± 11% increase; both $p < 0.05$, Wilcoxon paired test), while rise times were insignificantly lengthened (21 ± 9% increase) (Fig. 4C). However, steady-state synaptic depression was unaffected by cyclothiazide (Fig. 4B, 50 Hz data shown). These data indicate that AMPA receptor desensitization does not contribute to short-term plasticity at this synapse.

Receptor saturation is another possible cause of changes in postsynaptic glutamate sensitivity (Foster et al., 2002; Harrison and Jahr, 2003). We reduced saturation by applying the low-affinity glutamate receptor competitive antagonist γ-D-glutamyl glycine (γ-DGG, 2 mM; Fig. 4D) (Foster et al., 2005; Liu et al., 1999). As expected, γ-DGG reduced EPSC amplitude (to 28 ± 3% of original value, $p < 0.05$, Wilcoxon paired test, n = 6), while leaving synaptic kinetics intact (Fig. 4D, F). However, there was no change in the amplitude of steady-state depression (Fig. 4E, 50 Hz data shown). Together, these data demonstrate that neither saturation nor desensitization has a significant effect on frequency-independent steady-state depression at the vestibular afferent synapse, suggesting that postsynaptic receptor sensitivity to glutamate is stable across a wide range of presynaptic activity rates, and that the rate-invariance of this synapse is due to unusually stable presynaptic release probabilities.

In vivo, changes in head velocity are encoded as modulations of vestibular afferent firing rate. How is vestibular synaptic transmission affected by changes in afferent activity rates? To examine whether the afferent steady-state depression exhibited any sensitivity to transitions between input frequencies, we stimulated the vestibular nerve with two patterns of trains: 20 stimuli at 10 Hz to achieve steady state transmission followed by 20 stimuli at 50 Hz, or vice versa. In the example neuron shown, EPSCs depressed to about half the initial amplitude during the first 20 stimuli, and did not recover or depress further when the stimulation rate was changed in either direction (Fig. 5A). These findings are reflected in the group data (Figs. 5B, C).

The data presented thus far suggest that during physiological head movements, each vestibular afferent action potential evokes a fixed amount of transmitter release and postsynaptic current. This was examined more directly by challenging vestibular afferents with a naturalistic pattern of stimuli derived from combining measurements of mouse head movement (Beraneck et al., 2008) with vestibular afferent firing rates and sensitivity to head motion (Lasker et al., 2008; Yang and Hullar, 2007; see also Experimental Procedures). In response to a 5 s naturalistic stimulus, shown in Fig. 5D, EPSC amplitudes depressed rapidly to a plateau of 60% of the initial value for the duration of the stimulus (Fig. 5E). Within the steady state, evoked EPSC amplitude did not depend on stimulus interval (Fig. 5F). These data stand in contrast to findings at the hippocampal CA3 to CA1 synapse, where physiological patterns of activity drive rapid synaptic facilitation, resulting in small EPSCs during periods of quiescence but large responses during bursts of activity (Klyachko and Stevens, 2006). Instead, during physiological modulation of vestibular afferent firing rates, synaptic amplitudes are rate-invariant.

Given the high constant firing rates of vestibular afferents, the responses to trains of constant and naturalistic stimuli indicate that afferent synapses operate within a regime of steady-state depression. If transmission were to recover rapidly from depression, EPSC amplitude would no longer be constant. To examine the timecourse of recovery from depression, vestibular afferents were stimulated with 20-pulse conditioning trains at 10, 50, or 100 Hz, followed by a test pulse some variable time later (Fig. 6A). At long intervals (> 200 ms), EPSC recovery was best fit by a single exponential with a time constant of ~2 s for all three conditioning trains (Fig. 6B). However, over shorter intervals (10–100 ms), EPSCs did not recover in amplitude

(Fig. 6C; 50 Hz conditioning train). Furthermore, although EPSC recovery at many synapses includes a fast component that is diminished by additional slow Ca buffering (Dittman and Regehr, 1998;Yang and Xu-Friedman, 2008), application of 100 μM EGTA-AM had no effect on EPSC recovery at any interval (Fig. 6C, D).

The data presented thus far demonstrate that the synaptic charge transfer per unit time at the vestibular nerve synapse onto different types of vestibular nucleus neurons is linearly related to presynaptic activity rates. While it is known that the relationship between injected current and firing rate is linear in MVN neurons (du Lac and Lisberger, 1995; Fig. 7A), it is not known whether synapses are also capable of driving linear increases in firing rate in the face of changes in postsynaptic driving force. To evaluate the relationship between pre- and post-synaptic firing rates, responses of MVN neurons to 1 s of synaptic stimulation over a range of frequencies were recorded in current clamp. DC depolarizing or hyperpolarizing current was injected into MVN neurons to maintain a baseline firing rate of ~10 spikes/s, simulating the low end of *in vivo* firing rates (Beraneck and Cullen, 2007). As shown in Fig. 7B for an example neuron, synaptic stimulation at 20 and 100 Hz for 1 s evoked increases in postsynaptic spiking, with the associated firing rates plotted in Fig. 7C. Over all afferent stimulation rates tested, this MVN neuron responded to increases in synaptic input frequency with linear increases in firing rate, up through presynaptic stimulation rates of 150 Hz (Fig. 7D).

Stimulation of vestibular afferents onto both YFP-16 and GIN neurons elicited highly linear firing rate responses across stimulation rates ranging from 20–150 Hz (YFP-16, median R^2 = 0.948; GIN, 0.978) (Fig. 7E). At 200 Hz, there was typically a slight to moderate drop in response amplitude, as predicted from the greater synaptic depression observed at that stimulation frequency in voltage clamp (Fig. 3D). The synaptic gain was variable across neurons, as expected due to differences in synapse amplitude, depression profile, and postsynaptic membrane properties (YFP-16, median = 0.17 spikes/Hz; GIN, 0.09; $p = 0.09$, Wilcoxon unpaired test) (Fig. 7F). Blocking NMDA receptors with APV had no effect on synaptic gain (post/pre = 1.04) or linearity (post/pre = 0.96; data not shown, n = 3 YFP-16 neurons). In all but one cell tested, the gain was less than 1, indicating that several EPSPs summed temporally in a linear fashion, regardless of the frequency of afferent stimulation. Thus, vestibular nerve activity can drive linear increases in firing rate in both GABAergic and nonGABAergic neurons without relying on one-to-one calyceal connections.

Discussion

This study demonstrates that the excellent performance of the VOR is supported by a linear transformation from presynaptic to postsynaptic firing rate at the first central synapse in the vestibular system. Vestibular afferent stimulation evoked EPSCs in vestibular nucleus neurons that depressed rapidly to a maintained steady state amplitude which, within the behaviorally relevant range of afferent firing rates, did not depend on stimulus frequency or pattern. As a consequence, charge transfer across vestibular afferent synapses scaled linearly with stimulus frequency. The linearity evidenced at the synaptic level was preserved postsynaptically by linear current summation and spike generation. Neither postsynaptic sensitization nor receptor saturation affected the initial depression or steady-state transmission, pointing to a remarkable capacity for frequency-independent transmitter release by vestibular nerve afferent synapses.These results show that vestibular afferent synapses are well tuned to meet the demands of the stabilization system, in which head motion must be linearly matched by compensatory eye and body movement.

Rapid synaptic kinetics

The short latency of the VOR depends on rapid information transfer within a trisynaptic circuit. EPSCs from vestibular afferents exhibit swift rise and fall times (Fig. 2), resulting in no

appreciable summation of synaptic currents arriving at intervals as brief as 10 ms (Fig. 2 and Fig 3). The absence of effect of D-APV on postsynaptic firing responses to afferent stimulation indicates that NMDA receptor mediated current, which would broaden the EPSC, plays little role at mature ages. Thus, the majority of synaptic transmission at this site appears to be mediated by AMPA receptors. Rapid EPSC rise and fall times help keep postsynaptic depolarization brief, allowing for fast modulation of postsynaptic firing rate and rapid processing of sensory information.

Sustained history-independent release

Two features of the vestibular synaptic steady-state response are noteworthy: its sustained function even at high frequencies; and its fixed amplitude across a 30-fold range of firing rates. In the brainstem and cerebellum, baseline firing rates often exceed those of cerebral cortical regions, and several types of synapses exhibit the capacity for prolonged high-frequency transmission, such as the Purkinje cell output to target neurons in the deep cerebellar nuclei (Telgkamp and Raman, 2002) and the mossy fiber input to cerebellar granule cells (Saviane and Silver, 2006). At the Purkinje cell synapse, multiple release sites with low release probabilities permit robust transmission even at high frequencies (Telgkamp et al., 2004). Vestibular afferents may express similar specializations, although no studies have addressed this directly (Sato and Sasaki, 1993)

The finding that steady-state vestibular synaptic amplitudes are constant across a wide range of input frequencies contrasts with findings at excitatory cortical synapses, in which depression deepens as stimulation frequency increases (Abbott et al., 1997). What is the basis of this unusual property of vestibular transmission? We find that postsynaptic changes in glutamate sensitivity, in the form of AMPA receptor saturation and desensitization, contribute to neither the profile of short-term synaptic depression nor its frequency-independence (Fig. 4). Activity-dependent relief of polyamine block at calcium-permeable AMPA receptors (Rozov and Burnashev, 1999) is unlikely to contribute to depression because vestibular afferent synaptic properties are unchanged after ~1 hr patch recording without intracellular polyamines (data not shown). These results indicate that steady-state transmission derives from the ability of presynaptic terminals to release a constant quantity of transmitter following each action potential.

How does the range of frequency-independent release correspond to *in vivo* firing rates? Vestibular afferents encode head velocity via modulations around baseline firing rates (Goldberg and Fernandez, 1971). The high sensitivity and relatively low baseline firing rate of some mouse vestibular afferents make them susceptible to cutoff, or periods of no firing, during head movements that exceed 100 deg/s (Lasker et al., 2008; Yang and Hullar, 2007). However, estimations of head movement statistics in freely running mice from video (Beraneck et al., 2008) and gyroscopic (J. Moore, personal communication) analyses indicate that such rapid head velocities occur infrequently and typically last no more than 200 ms, equivalent to a rate of ~5 spikes/s. Although the most sensitive afferent fibers exhibiting the highest spontaneous rates could increase firing rates transiently up to 200 Hz during rapid head movements, firing rates of the majority of afferents would typically remain below 100 spikes/s. Thus, under behaviorally relevant conditions, the predominant firing rate range of vestibular afferents is 5 – 100 Hz, which matches the frequency-independent range of synaptic transmission.

Within the physiologically relevant regime of maintained afferent discharge, our results indicate that each action potential evokes the same amount of transmitter release. Multiple presynaptic factors control transmitter release, including magnitude of Ca^{2+} influx, sensitivity of the release machinery to Ca^{2+}, and vesicle availability (Zucker and Regehr, 2002). After prolonged periods of silence (which do not normally occur *in vivo*), presynaptic release exhibits

a high initial amplitude, which then diminishes rapidly in the face of repeated stimuli. This short term depression could reflect changes in Ca^{2+} influx, Ca^{2+}-triggered biochemical changes, or depletion of a slowly-replenished pool of vesicles. Consistent with the latter hypothesis, synaptic amplitude recovers with a slow timecourse after stimulus trains (Fig. 6). At both the climbing fiber synapse and the calyx of Held, recovery from depression is best described by a combination of fast and slow processes, with the fast process being sensitive to application of EGTA-AM (Dittman and Regehr, 1998; Yang and Xu-Friedman, 2008). In contrast, recovery from depression at the vestibular afferent synapse is well described by a single exponential and does not occur at all for short intervals of < 100 ms (Fig. 6). Furthermore, synaptic responses at all intervals were resistant to the effects of buffering residual Ca^{2+} with intracellular EGTA. In the simplest model for steady-state transmission consistent with our results, each afferent action potential triggers influx of a fixed amount of Ca^{2+}, which evokes a cycle of coordinated vesicle release and replenishment before being rapidly cleared from the presynaptic terminal. Given the maintained high firing rates at this synapse and the energetic costs of vesicle recycling, we suggest that vestibular afferents contain multiple release sites, each with low probability of release, such has been observed at Purkinje cell synapses (Telgkamp et al., 2004). Ultrastructural studies of the vestibular afferent synapse will be useful in evaluating this hypothesis.

Linear signal processing throughout the vestibular system

Eye movements compensate almost perfectly for head movements in the mouse (Fig. 1) as in other species (Robinson, 1981). Notably, each stage of vestibulo-ocular reflex processing examined thus far has been shown to be linear, including the transformation from head velocity to firing rates in both vestibular nerve and vestibular nucleus neurons (Goldberg and Fernandez, 1971;Shimazu and Precht, 1965), as well as between oculomotor neuronal activity and eye velocity (Skavenski and Robinson, 1973). In primates, the firing range of vestibular afferents is double that in mice (Lasker et al., 2008;Yang and Hullar, 2007). Limitations in rate-invariant transmission might account for some of the nonlinearities observed in the primate VOR during rapid accelerations of the head (Minor et al., 1999).

Because our data provide a plausible physiological framework for linear synaptic transmission, we suggest that EPSC amplitudes may also be rate-invariant at other connections in the vestibular system, such as those from vestibular nucleus neurons to oculomotor neurons. Indeed, recent work supports this prediction at the vestibular nucleus neuron synapse onto granule cells in the cerebellum. At this synapse, EPSC frequency, but not amplitude, is modulated during head movement such that the total charge transfer is linearly related to head velocity (Arenz et al., 2008). Interestingly, the short term dynamics of mossy fiber synapses are affected by blockers of saturation and desensitization (Saviane and Silver, 2006), in contrast to the dynamics of primary afferent synapses onto vestibular nucleus neurons (Fig. 4). It remains to be determined whether these mechanistic differences compromise the ability of granule cells to fire linearly over a wide range of mossy fiber input rates, as we demonstrate in vestibular nucleus neurons (Fig. 7).

Ongoing activity promotes linearity

A salient property of vestibular circuits is that neurons fire continuously even in the absence of head motion. Operating around high baseline firing rates confers three advantages. First, sensory stimuli can be encoded as modulations in firing rate, providing a opportunity for bidirectional encoding of information--in this case, both increases and decreases in head velocity. Second, postsynaptic neurons do not need to be depolarized from a hyperpolarized resting membrane potential, but instead are maintained in a voltage range close to threshold, minimizing the latency from synaptic input to postsynaptic firing. Third, silent neurons often exhibit nonlinearities in synaptic summation, because small inputs may not affect postsynaptic

firing while large inputs may drive dendritic and somatic spiking (e.g., Carter et al., 2007; Gasparini and Magee, 2006). Maintaining high firing rates may be one measure by which vestibular circuit neurons avoid these nonlinearities.

Functional implications

At synapses that exhibit reliable transmission, such as auditory afferents or the neuromuscular junction, a flood of neurotransmitter release guarantees a successful postsynaptic spike. Vestibular afferents do not achieve linearity through one-to-one connections such as these, but instead rely on a combination of frequency-independent release and linear postsynaptic processing (Fig. 7). Why? We suggest that the major advantage of the vestibular solution is its flexibility. Calyceal transmission necessarily limits the prospects for modifiability. Vestibular nucleus neurons integrate information from visual and proprioceptive sources, in addition to direct and indirect vestibular sensory inputs (Angelaki and Cullen, 2008). Furthermore, the VOR is bidirectionally plastic throughout life, and one candidate locus of memory storage is the vestibular afferent input (Broussard and Kassardjian, 2004;Gittis and du Lac, 2006). It will be of great interest to determine whether the synaptic strengths of vestibular afferents can be altered without compromising their distinctive frequency-independence.

Experimental Procedures

Behavioral testing

Linearity of the vestibulo-ocular reflex (VOR) was assessed in 6 C57/Bl6 mice at ages of 2–4 months as detailed (Faulstich et al., 2004). Mice were secured in a padded restraining tube with a post which had been affixed surgically to the head 3 days prior. The restraining tube was held in the middle of a turntable (Biomedical Engineering, NY, USA) such that the midpoint of the interaural axis was centered and tilted to align horizontal semicircular canals with earth horizontal (Calabrese and Hullar, 2006; Vidal et al., 2004). Eye movements were acquired with an infrared video camera mounted on the turntable which measured pupillary position and size and corneal reflection (RK-726I; Iscan). Pupil dilation was minimized with a 0.5% physostigmine solution applied 30–60 min prior to recordings. The VOR was evoked by rotating the turntable sinusoidally at a frequency of 1Hz with peak-to-peak amplitudes ranging from 1.25 to 50°, resulting in peak stimulus velocities from 3.9 to 157 °/s. Eye movements were evoked in complete darkness, sampled at 60 Hz, and calibrated as described (Stahl, 2002; Stahl et al., 2000). Analyses of eye movements were performed in the velocity domain after digitally differentiating table and eye position traces, removing saccadic intrusions with a velocity threshold algorithm, and manually excluding traces with motion artifacts. Peak velocities were calculated from sinusoidal fits to table and eye velocity.

Physiology

Two transgenic lines of mice were used for synaptic physiology: YFP-16 (Feng et al., 2000), in which glutamatergic and glycinergic neurons in the MVN are fluorescently labeled; and GIN, in which a subset of GABAergic MVN neurons are fluorescently labeled (Bagnall et al., 2007; Oliva et al., 2000). Anatomical, physiological, and neurochemical evidence indicates that neurons labeled in the YFP-16 line are projection neurons, while neurons labeled in the GIN line are local neurons whose axons remain within the bilateral MVN (Bagnall et al., 2007; Epema et al., 1988; Holstein, 2000). Mice aged 15–25 days postnatal (mean, P21 ± 0.3) were deeply anesthetized with Nembutal and decapitated. After rapid dissection in ice cold Ringer's solution (in mM: 124 NaCl, 5 KCl, 1.3 $MgSO_4$, 26 $NaHCO_3$, 2.5 $CaCl_2$, 1 NaH_2PO_4), 250 – 400 μm thick slices were cut on a DSK DTK-1500E or Leica VT1000S vibratome and allowed to recover at 34 °C for 30 min. Slices rested at room temperature before being transferred to a recording chamber and perfused with carbogenated Ringer's containing

1–10 μM strychnine and 100 μM picrotoxin at 34 °C. All experiments were carried out in accordance with the standards of the Salk Institute IACUC.

Patch pipettes were pulled from flame-polished glass (Warner) with resistances of ~2–4 MΩ. Pipette internal solution contained (in mM) 140 K gluconate, 10 HEPES, 8 NaCl, 0.1 EGTA, 2 Mg-ATP, 0.3 Na_2-GTP. In the experiments involving application of γ-D-glutamyl glycine (γ-DGG), the K gluconate was replaced with Cs gluconate, and 1 mM QX-314 was added to the internal solution. Neurons were visualized with epifluorescence through a GFP filter as well as under infrared differential interference contrast illumination with Nomarski optics. A bipolar concentric stimulating electrode (FHC, Maine) was placed on the vestibular nerve lateral to the vestibular complex and controlled via two Isoflex stimulus isolation units (AMPI, Israel). A biphasic pulse, consisting of two 100 μs pulses of opposite polarity with a 100 μs interval, was delivered to the electrode to avoid charge build-up during high frequency trains.

Data were acquired with a Multiclamp 700B low-pass filtering at 6–10 kHz for voltage clamp and 10 kHz for current clamp. Data were digitized at 40 kHz with an ITC-16 or 18 (InstruTECH). House-written code in Igor 5 was used for acquisition and analysis. Recordings were discarded if series resistance, tested with a small hyperpolarizing square pulse, exceeded 20 MΩ. 5–10 sweeps (10–30 s interstimulus interval) of each stimulus train were averaged together. Neurons were usually held in current clamp between epochs of recording in voltage clamp; in two example traces (Fig. 5) a small (~25 pA) drift in holding current has been subtracted for display purposes.

Because vestibular nerve afferents are heterogeneous with respect to diameter and myelination, conduction velocities vary across the afferent population. As a result, in many EPSCs an inflection point was visible in the rise and/or decay, representing the arrival of several different synaptic currents at slightly different latencies. All such EPSCs were monosynaptic, based on their latency (< 2 ms) and on the fact that they did not disappear during manipulation of external divalent ions intended to eliminate disynaptic activation (to 1 mM Ca^{2+}, 2.8 mM Mg^{2+}; or to 4 mM Ca^{2+}, 4 mM Mg^{2+}, data not shown). There was no clear relationship between stimulation intensity and the recruitment of these longer- or shorter- latency EPSC components. Because of the impossibility of studying these components systematically, we analyzed EPSC decay kinetics with a 90–10% or 80–20% fall time measure, rather than with exponential fits. During recordings, stimulation intensity was adjusted to produce a reliable EPSC, normally in the range of 1.5 – 3x the threshold intensity. During voltage clamp, the postsynaptic cell was clamped at −75 mV to isolate primarily an AMPA-mediated response. Firing rates are reported as the average of the reciprocal of the inter-spike interval, and were averaged across the entire 1 s of synaptic stimulation.

Statistical tests were done with KaleidaGraph 3.6 (Synergy Software) and are reported as mean ± SEM except as noted. Synthesized Cs gluconate was a gift of Dr. Court Hull. Chemicals were purchased from Sigma (St. Louis MO), with the exception of γ-DGG and cyclothiazide (Tocris, Bristol, UK) and EGTA-AM (Invitrogen). EGTA-AM was dissolved in DMSO (final concentration 0.05 – 0.1%). Following baseline trials, it was washed into the bath for 5 min prior to testing.

Naturalistic stimuli

Head velocity in freely locomoting mice was measured with a small head-mounted gyroscope which detected yaw velocity with bandwidth of 80 Hz (Analog Devices). Head movement signals were measured during 30 s epochs while mice were running in their home cages. The statistics of the head velocity data corresponded well with those reported during video analysis of mouse head movement (Beraneck et al., 2008); head movements reaching velocities in excess of 100 °/s were observed less than 15% of the time, and epochs of these fast head

movements lasted < 200 ms. A naturalistic stimulus was constructed by scaling a representative 5 s head velocity trace by 0.2, the average sensitivity of mouse regular and irregular type vestibular afferents, and assuming a baseline firing rate of 36 Hz, near the average for irregular afferents (Lasker et al., 2008; Yang and Hullar, 2007). This pattern was developed to maximize the possibility of uncovering nonlinearities of synaptic transmission in the low firing rate range.

Acknowledgments

The authors thank Drs. Massimo Scanziani, Edward B. Han, and Takashi Kodama for valuable discussions, Dr. Gabe J. Murphy for pilot physiology, and Jeffrey Moore for mouse head movement data. This work was supported by the Howard Hughes Medical Institute, NIH EY-11027, and a National Science Foundation Graduate Research Fellowship to M.W.B.

References

Abbott LF, Regehr WG. Synaptic computation. Nature 2004;431:796–803. [PubMed: 15483601]

Abbott LF, Varela JA, Sen K, Nelson SB. Synaptic depression and cortical gain control. Science 1997;275:220–224. [PubMed: 8985017]

Angelaki DE, Cullen KE. Vestibular system: the many facets of a multimodal sense. Annu Rev Neurosci 2008;31:125–150. [PubMed: 18338968]

Arenz A, Silver RA, Schaefer AT, Margrie TW. The contribution of single synapses to sensory representation in vivo. Science 2008;321:977–980. [PubMed: 18703744]

Babalian A, Vibert N, Assie G, Serafin M, Muhlethaler M, Vidal PP. Central vestibular networks in the guinea-pig: functional characterization in the isolated whole brain in vitro. Neuroscience 1997;81:405–426. [PubMed: 9300431]

Bagnall MW, Stevens RJ, du Lac S. Transgenic mouse lines subdivide medial vestibular nucleus neurons into discrete, neurochemically distinct populations. J Neurosci 2007;27:2318–2330. [PubMed: 17329429]

Beraneck M, Cullen KE. Activity of vestibular nuclei neurons during vestibular and optokinetic stimulation in the alert mouse. J Neurophysiol 2007;98:1549–1565. [PubMed: 17625061]

Beraneck M, McKee JL, Aleisa M, Cullen KE. Asymmetric recovery in cerebellar-deficient mice following unilateral labyrinthectomy. J Neurophysiol 2008;100:945–958. [PubMed: 18509072]

Broussard DM, Kassardjian CD. Learning in a simple motor system. Learn Mem 2004;11:127–136. [PubMed: 15054127]

Calabrese DR, Hullar TE. Planar relationships of the semicircular canals in two strains of mice. J Assoc Res Otolaryngol 2006;7:151–159. [PubMed: 16718609]

Carter AG, Soler-Llavina GJ, Sabatini BL. Timing and location of synaptic inputs determine modes of subthreshold integration in striatal medium spiny neurons. J Neurosci 2007;27:8967–8977. [PubMed: 17699678]

Dittman JS, Regehr WG. Calcium dependence and recovery kinetics of presynaptic depression at the climbing fiber to Purkinje cell synapse. J Neurosci 1998;18:6147–6162. [PubMed: 9698309]

du Lac S, Lisberger SG. Membrane and firing properties of avian medial vestibular nucleus neurons in vitro. J Comp Physiol [A] 1995;176:641–651.

Epema AH, Gerrits NM, Voogd J. Commissural and intrinsic connections of the vestibular nuclei in the rabbit: a retrograde labeling study. Exp Brain Res 1988;71:129–146. [PubMed: 2458274]

Faulstich BM, Onori KA, du Lac S. Comparison of plasticity and development of mouse optokinetic and vestibulo-ocular reflexes suggests differential gain control mechanisms. Vision Res 2004;44:3419–3427. [PubMed: 15536010]

Feng G, Mellor RH, Bernstein M, Keller-Peck C, Nguyen QT, Wallace M, Nerbonne JM, Lichtman JW, Sanes JR. Imaging neuronal subsets in transgenic mice expressing multiple spectral variants of GFP. Neuron 2000;28:41–51. [PubMed: 11086982]

Foster KA, Crowley JJ, Regehr WG. The influence of multivesicular release and postsynaptic receptor saturation on transmission at granule cell to Purkinje cell synapsesq. J Neurosci 2005;25:11655–11665. [PubMed: 16354924]

Foster KA, Kreitzer AC, Regehr WG. Interaction of postsynaptic receptor saturation with presynaptic mechanisms produces a reliable synapse. Neuron 2002;36:1115–1126. [PubMed: 12495626]

Furman JM, O'Leary DP, Wolfe JW. Dynamic range of the frequency response of the horizontal vestibulo-ocular reflex of the alert rhesus monkey. Acta Otolaryngol 1982;93:81–91. [PubMed: 7064700]

Gasparini S, Magee JC. State-dependent dendritic computation in hippocampal CA1 pyramidal neurons. J Neurosci 2006;26:2088–2100. [PubMed: 16481442]

Gittis AH, du Lac S. Intrinsic and synaptic plasticity in the vestibular system. Curr Opin Neurobiol 2006;16:385–390. [PubMed: 16842990]

Goldberg JM, Fernandez C. Physiology of peripheral neurons innervating semicircular canals of the squirrel monkey. I. Resting discharge and response to constant angular accelerations. J Neurophysiol 1971;34:635–660. [PubMed: 5000362]

Harrison J, Jahr CE. Receptor occupancy limits synaptic depression at climbing fiber synapses. J Neurosci 2003;23:377–383. [PubMed: 12533597]

Highstein SM, Rabbitt RD, Holstein GR, Boyle RD. Determinants of spatial and temporal coding by semicircular canal afferents. J Neurophysiol 2005;93:2359–2370. [PubMed: 15845995]

Holstein, GR. Inhibitory amino acid transmitters in the vestibular nuclei. In: Beitz, AJ.; Anderson, JH., editors. Neurochemistry of the vestibular system. Florida: CRC Press; 2000. p. 143-162.

Huterer M, Cullen KE. Vestibuloocular reflex dynamics during high-frequency and high-acceleration rotations of the head on body in rhesus monkey. J Neurophysiol 2002;88:13–28. [PubMed: 12091529]

Huwe JA, Peterson EH. Differences in the brain stem terminations of large- and small-diameter vestibular primary afferents. J Neurophysiol 1995;74:1362–1366. [PubMed: 7500159]

Isaacson JS, Walmsley B. Amplitude and time course of spontaneous and evoked excitatory postsynaptic currents in bushy cells of the anteroventral cochlear nucleus. J Neurophysiol 1996;76:1566–1571. [PubMed: 8890276]

Klyachko VA, Stevens CF. Excitatory and feed-forward inhibitory hippocampal synapses work synergistically as an adaptive filter of natural spike trains. PLoS Biol 2006;4:e207. [PubMed: 16774451]

Lasker DM, Han GC, Park HJ, Minor LB. Rotational Responses of Vestibular-Nerve Afferents Innervating the Semicircular Canals in the C57BL/6 Mouse. J Assoc Res Otolaryngol. 2008

Lewis MR, Phelan KD, Shinnick-Gallagher P, Gallagher JP. Primary afferent excitatory transmission recorded intracellularly in vitro from rat medial vestibular neurons. Synapse 1989;3:149–153. [PubMed: 2538943]

Lisberger SG, Miles FA. Role of primate medial vestibular nucleus in long-term adaptive plasticity of vestibuloocular reflex. J Neurophysiol 1980;43:1725–1745. [PubMed: 6967953]

Liu G, Choi S, Tsien RW. Variability of neurotransmitter concentration and nonsaturation of postsynaptic AMPA receptors at synapses in hippocampal cultures and slices. Neuron 1999;22:395–409. [PubMed: 10069344]

Minor LB, Lasker DM, Backous DD, Hullar TE. Horizontal vestibuloocular reflex evoked by high-acceleration rotations in the squirrel monkey. I. Normal responses. J Neurophysiol 1999;82:1254–1270. [PubMed: 10482745]

Oliva AA Jr, Jiang M, Lam T, Smith KL, Swann JW. Novel hippocampal interneuronal subtypes identified using transgenic mice that express green fluorescent protein in GABAergic interneurons. J Neurosci 2000;20:3354–3368. [PubMed: 10777798]

Pastor AM, de la Cruz RR, Baker R. Characterization and adaptive modification of the goldfish vestibuloocular reflex by sinusoidal and velocity step vestibular stimulation. J Neurophysiol 1992;68:2003–2015. [PubMed: 1491254]

Pulaski PD, Zee DS, Robinson DA. The behavior of the vestibulo-ocular reflex at high velocities of head rotation. Brain Res 1981;222:159–165. [PubMed: 7296263]

Robinson DA. Adaptive gain control of vestibuloocular reflex by the cerebellum. J Neurophysiol 1976;39:954–969. [PubMed: 1086347]

Robinson DA. The use of control systems analysis in the neurophysiology of eye movements. Annu Rev Neurosci 1981;4:463–503. [PubMed: 7013640]

Rozov A, Burnashev N. Polyamine-dependent facilitation of postsynaptic AMPA receptors counteracts paired-pulse depression. Nature 1999;401:594–598. [PubMed: 10524627]

Sato F, Sasaki H. Morphological correlations between spontaneously discharging primary vestibular afferents and vestibular nucleus neurons in the cat. J Comp Neurol 1993;333:554–566. [PubMed: 8370817]

Saviane C, Silver RA. Fast vesicle reloading and a large pool sustain high bandwidth transmission at a central synapse. Nature 2006;439:983–987. [PubMed: 16496000]

Scudder CA, Fuchs AF. Physiological and behavioral identification of vestibular nucleus neurons mediating the horizontal vestibuloocular reflex in trained rhesus monkeys. J Neurophysiol 1992;68:244–264. [PubMed: 1517823]

Shimazu H, Precht W. Tonic and kinetic responses of cat's vestibular neurons to horizontal angular acceleration. J Neurophysiol 1965;28:991–1013. [PubMed: 5295930]

Skavenski AA, Robinson DA. Role of abducens neurons in vestibuloocular reflex. J Neurophysiol 1973;36:724–738. [PubMed: 4197340]

Stahl JS. Calcium channelopathy mutants and their role in ocular motor research. Ann N Y Acad Sci 2002;956:64–74. [PubMed: 11960794]

Stahl JS, van Alphen AM, De Zeeuw CI. A comparison of video and magnetic search coil recordings of mouse eye movements. J Neurosci Methods 2000;99:101–110. [PubMed: 10936649]

Straka H, Dieringer N. Uncrossed disynaptic inhibition of second-order vestibular neurons and its interaction with monosynaptic excitation from vestibular nerve afferent fibers in the frog. J Neurophysiol 1996;76:3087–3101. [PubMed: 8930257]

Straka H, Dieringer N. Basic organization principles of the VOR: lessons from frogs. Prog Neurobiol 2004;73:259–309. [PubMed: 15261395]

Telgkamp P, Padgett DE, Ledoux VA, Woolley CS, Raman IM. Maintenance of high-frequency transmission at purkinje to cerebellar nuclear synapses by spillover from boutons with multiple release sites. Neuron 2004;41:113–126. [PubMed: 14715139]

Telgkamp P, Raman IM. Depression of inhibitory synaptic transmission between Purkinje cells and neurons of the cerebellar nuclei. J Neurosci 2002;22:8447–8457. [PubMed: 12351719]

Trussell LO, Zhang S, Raman IM. Desensitization of AMPA receptors upon multiquantal neurotransmitter release. Neuron 1993;10:1185–1196. [PubMed: 7686382]

Vidal PP, Degallaix L, Josset P, Gasc JP, Cullen KE. Postural and locomotor control in normal and vestibularly deficient mice. J Physiol 2004;559:625–638. [PubMed: 15243133]

von Gersdorff H, Borst JG. Short-term plasticity at the calyx of held. Nat Rev Neurosci 2002;3:53–64. [PubMed: 11823805]

Wong AY, Graham BP, Billups B, Forsythe ID. Distinguishing between presynaptic and postsynaptic mechanisms of short-term depression during action potential trains. J Neurosci 2003;23:4868–4877. [PubMed: 12832509]

Yang A, Hullar TE. The relationship of semicircular canal size to vestibular-nerve afferent sensitivity in mammals. J Neurophysiol. 2007

Yang H, Xu-Friedman MA. Relative roles of different mechanisms of depression at the mouse endbulb of held. J Neurophysiol 2008;99:2510–2521. [PubMed: 18367696]

Zucker RS, Regehr WG. Short-term synaptic plasticity. Annu Rev Physiol 2002;64:355–405. [PubMed: 11826273]

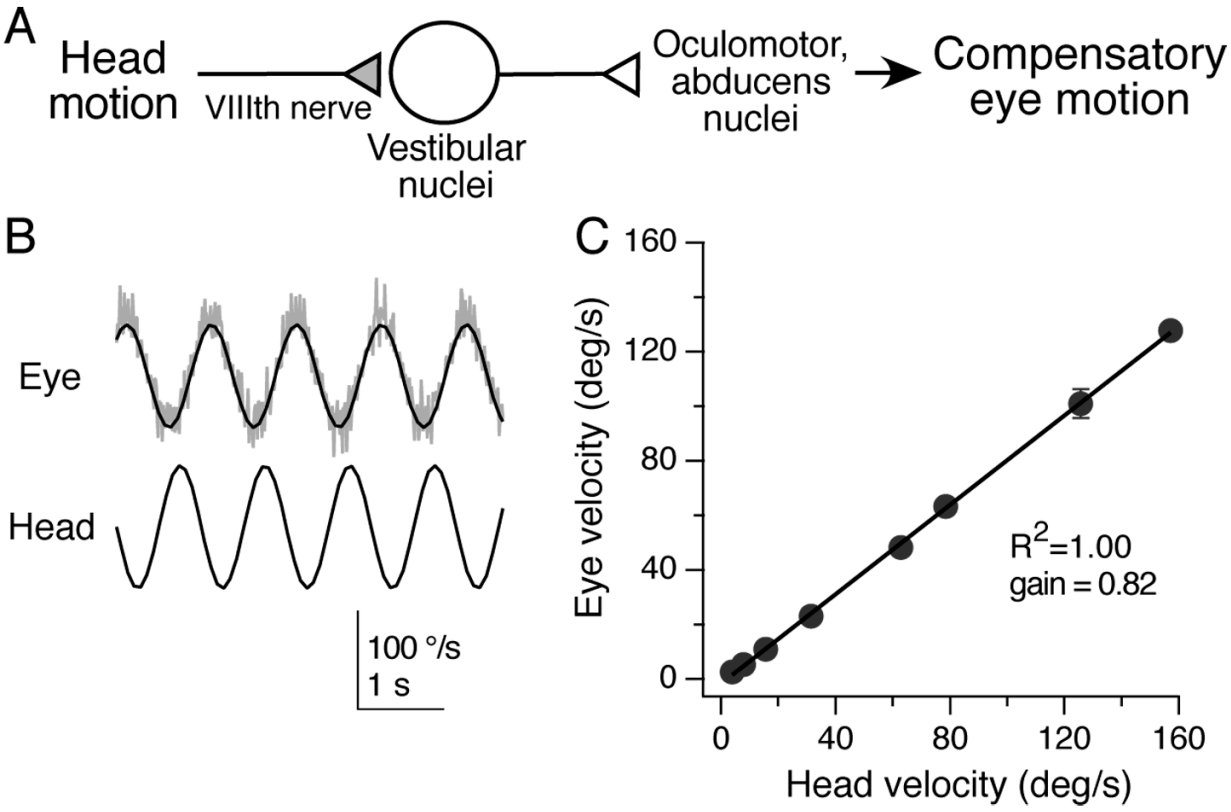

Figure 1. Linear relationship between head velocity and compensatory eye velocity

A, The basic circuitry of the vestibulo-ocular reflex; the vestibular nerve afferent synapse onto vestibular nucleus neurons (shaded) is the focus of this study. B, In the dark, mice were rotated sinusoidally in the horizontal plane at a frequency of 1 Hz. Example of eye and head velocity in one mouse. Instantaneous eye velocity is shown in gray, with sinusoidal fit in black. C, Summary data for six mice showing that eye velocity was a linear function of head motion at 1 Hz over a wide range of velocities. Error bars represent SD and in most cases are smaller than the symbols.

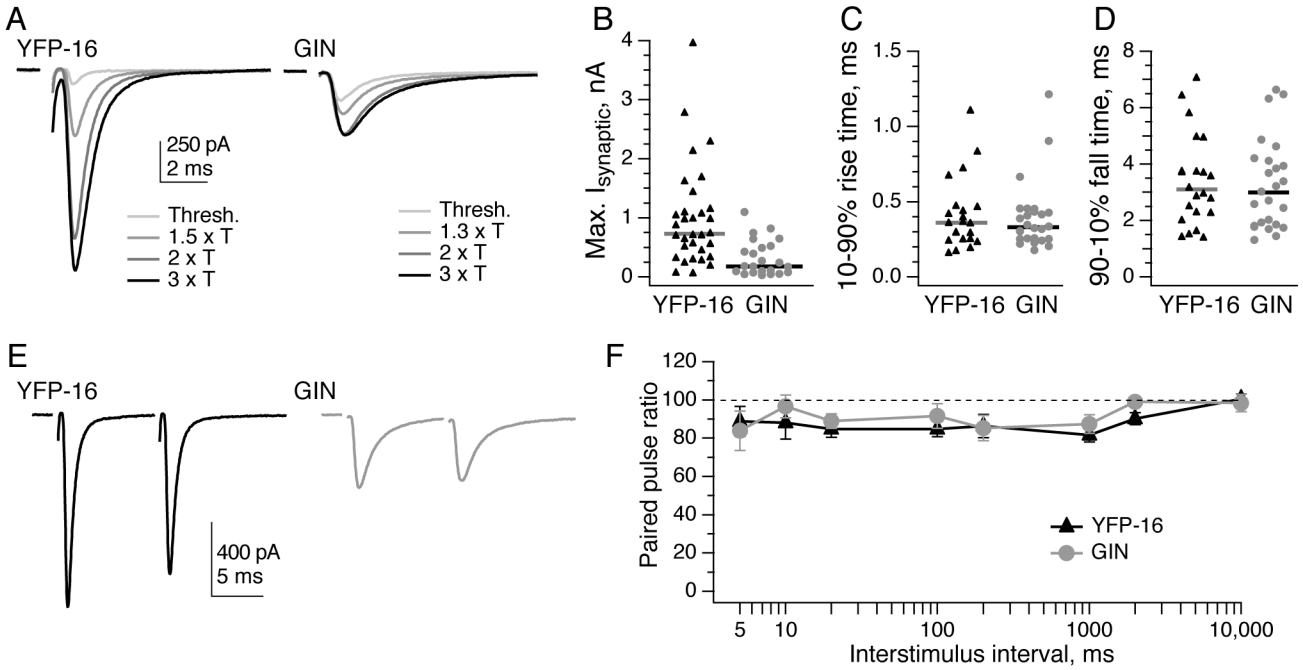

Figure 2. EPSCs from vestibular afferents exhibit rapid kinetics and little paired-pulse modulation

A, Example EPSCs resulting from increasing stimulation intensities of the vestibular nerve in slice preparation, recorded from neurons labeled in the YFP-16 line (left) and the GIN line (right). Stimulation artifacts are blanked for clarity. T = threshold stimulation intensity. B, The maximum EPSC amplitude that could be elicited in YFP-16 neurons was 3-fold higher than that in GIN neurons ($p < 0.0001$). Two YFP-16 neurons had maximal EPSCs of 5–6 nA (not shown for graphical clarity). C, EPSC 10–90% rise times are rapid both in YFP-16 neurons and GIN neurons. D, EPSC 90–10% decay times (see Experimental Procedures) are also swift in YFP-16 and GIN neurons. Kinetics were usually measured at 1.5–3x the threshold stimulation intensity. Horizontal bars represent medians. E, Paired pulse. Examples of EPSCs elicited at a 10 ms interval in a YFP-16 (left) and GIN (right) neuron. F, Summary of paired-pulse ratios (100*EPSC2/EPSC1) across interstimulus intervals from 5 ms to 10 s. EPSCs in both YFP-16 and GIN neurons depressed to ~85% of their original values at stimulus intervals from 5 ms to 1 s, with no history dependence visible at intervals of 10 s. N = 3–10 cells per data point. Data are shown as mean ± SEM in this and subsequent figures.

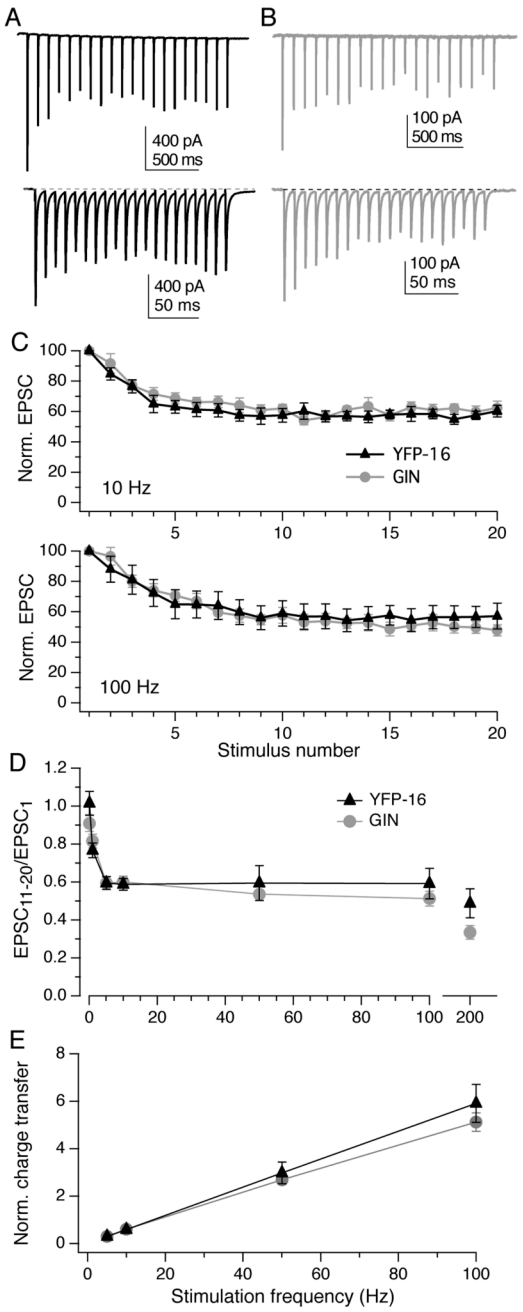

Figure 3. Trains of stimuli evoke frequency-independent steady-state depression

A, EPSCs measured in a YFP-16 neuron during vestibular nerve stimulation at 10 Hz (top) or 100 Hz (bottom). B, Same as A, GIN neuron. In both examples, EPSCs rapidly achieve a steady-state plateau of ~60% of the initial value, regardless of stimulation frequency. C, Population data from both YFP-16 (n = 8) and GIN neurons (n = 11) with trains of 20 stimuli elicited at 10 Hz. D, Population data from YFP-16 (n = 7) and GIN neurons (n = 8) with trains of 20 stimuli elicited at 100 Hz. D, Summary of the magnitude of steady-state depression, defined as the average of $EPSC_{11–20}$ divided by $EPSC_1$, across stimulation frequencies from 0.1 to 200 Hz. In the steady state, EPSC amplitude does not depend on stimulation frequency from 5 to 100 Hz in either YFP-16 or GIN neurons. E, Total charge transfer per second during

steady-state transmission increases linearly with increasing stimulation frequency ($R^2 = 1$ for both neuron types). Charge transfer was calculated as the average integrated area under the EPSC in steady state ($EPSC_{11–20}$), normalized to initial EPSC amplitude, and multiplied by the rate of stimulation.

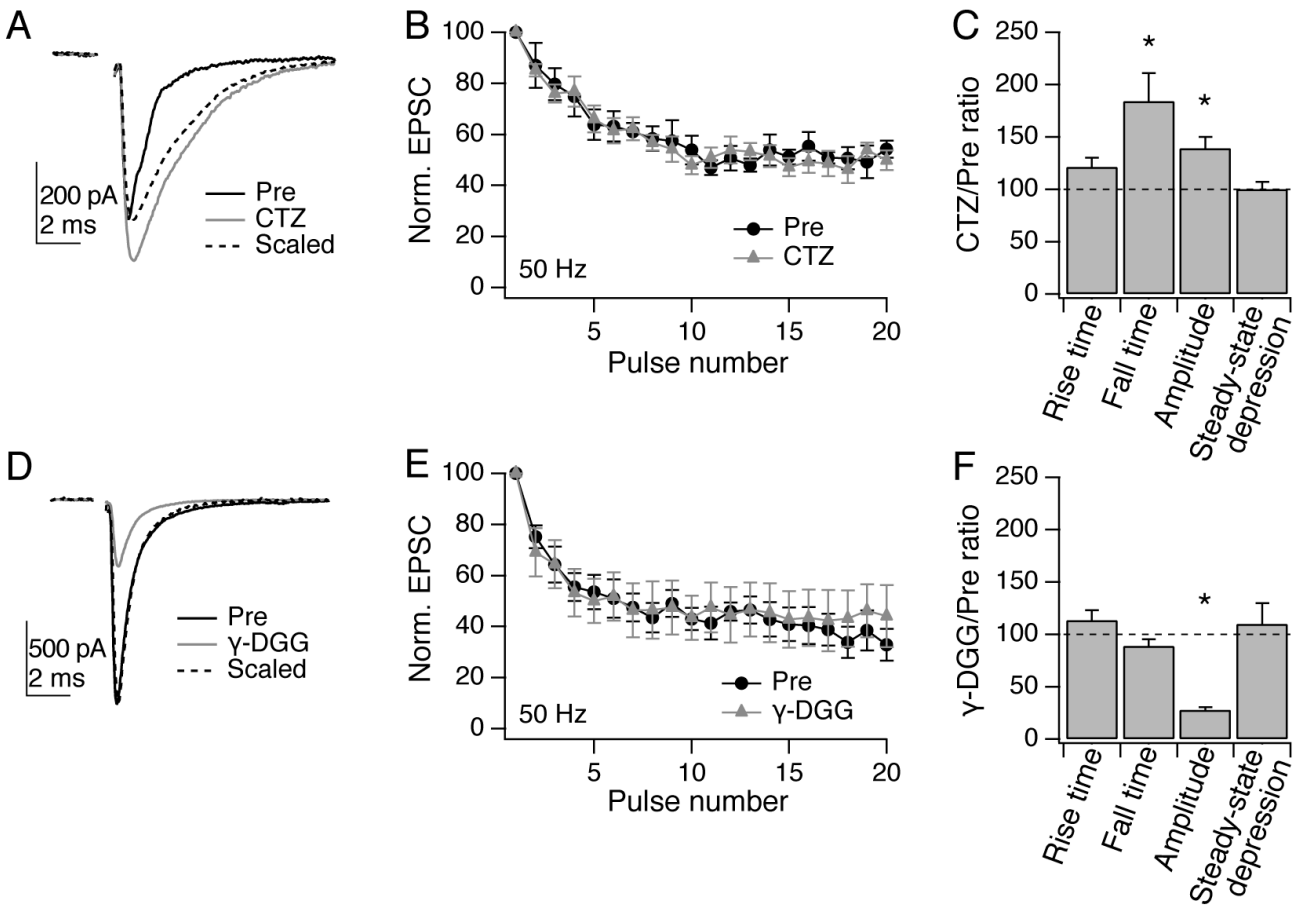

Figure 4. Postsynaptic receptor desensitization and saturation do not affect short-term plasticity

A, Example EPSC elicited by vestibular nerve stimulation in a YFP-16 neuron (black). Cyclothiazide (100 μm; gray) increased EPSC amplitude and slowed its decay, as is evident in the experimental trace peak-scaled to control (dotted line). B, No difference is seen in steady-state depression of synaptic currents in the presence of cyclothiazide at 50 Hz (shown) or other frequencies tested (n = 6). C, Summary of kinetics and steady-state depression across the population. The peak EPSC amplitude and the 80-20% decay time were both significantly increased by cyclothiazide (n = 6; $p < 0.05$). Steady-state depression, quantified as EPSC11-20/EPSC1, was unaffected. D, Example EPSC elicited in a YFP-16 neuron. γ-DGG (2 mM; gray) reduced EPSC amplitude without significantly affecting kinetics (scaled trace, dotted line). E, Reducing receptor saturation does not affect short-term depression at 50 Hz (shown) or other frequencies tested (n = 6). F, Summary of kinetics and steady-state depression across the population. EPSC amplitude was significantly reduced ($p < 0.05$) while other parameters were unaffected.

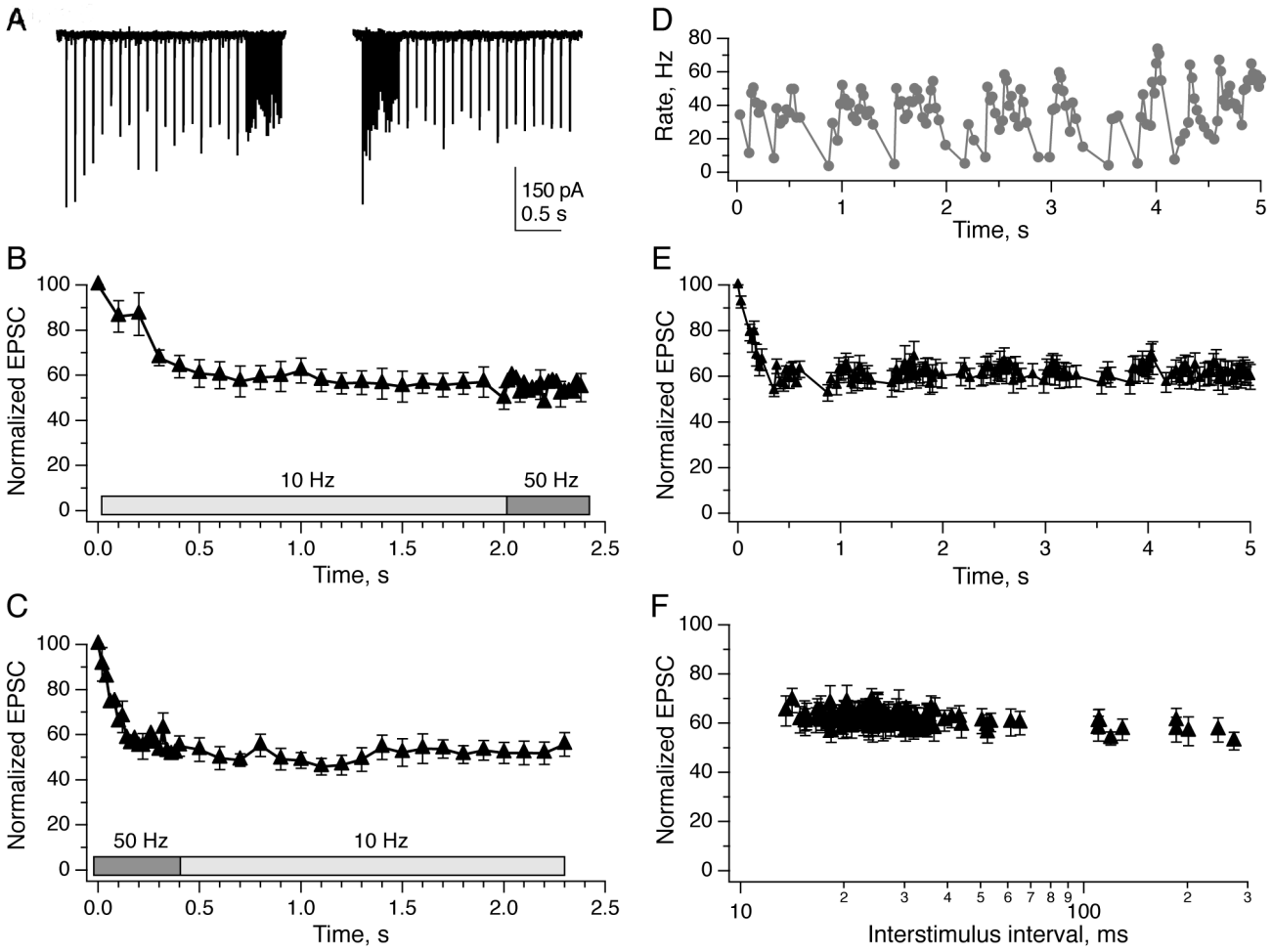

Figure 5. The amplitude of steady state transmission is not affected by changes in stimulation rate

A, Example EPSCs recorded in a YFP-16 neuron during vestibular afferent stimulation with 20 pulses at 10 Hz followed by 20 pulses at 50 Hz (left) and 50 Hz followed by 10 Hz (right). Group data indicate that EPSC amplitudes were not affected by stimulus shifts from 10 Hz to 50 Hz (B, n=8) or from 50 Hz to 10 Hz (C, n=9). D, Naturalistic stimulus train, displayed as instantaneous rate vs time, that approximates the firing pattern of a typical mouse vestibular afferent firing during head movements (see Experimental Procedures). E, Average EPSC responses to the naturalistic stimulus shown in D (n = 7). EPSC amplitude decreased rapidly to a steady state level that was not affected by instantaneous variations in stimulus rate. F, Replotting the data from E demonstrated that EPSC amplitude did not depend on interstimulus interval. The responses to the first five stimuli have been omitted from this plot for clarity.

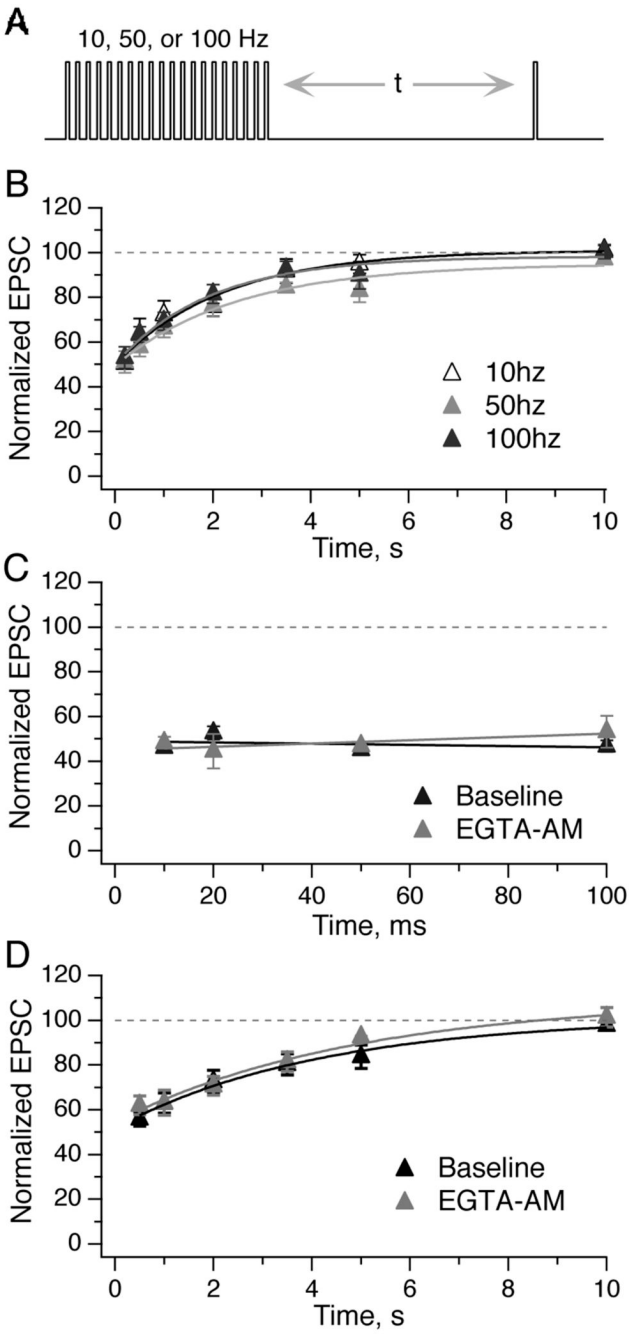

Figure 6. Recovery of EPSC amplitudes from depression is slow and monoexponential

A, Vestibular afferents were stimulated with conditioning trains of 20 pulses at 10, 50, or 100 Hz, followed by a test pulse at a variable time afterwards. B, Recovery from depression was best fit with a single exponential. The tau of recovery was similar across the three conditioning frequencies of 10, 50, and 100 Hz (2.2, 2.5, and 1.9 s respectively; n = 5). C, EPSCs did not recover in amplitude during shorter intervals (10–100 ms, all tested with 50 Hz conditioning train). Application of 100 μM EGTA-AM for 5 min had no effect on recovery (n = 4). D, EGTA-AM had no effect on the timecourse of recovery for longer test intervals (conditioning train, 50 Hz; n = 7).

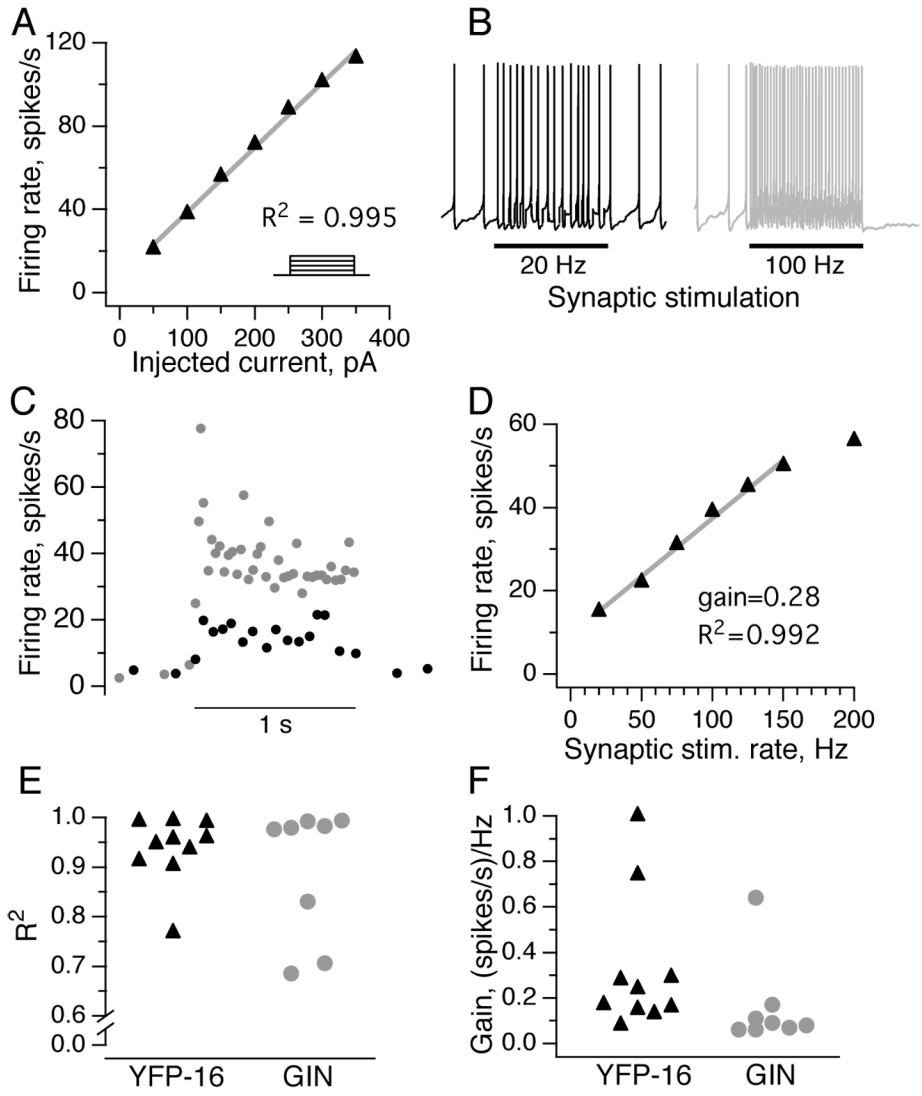

Figure 7. Injected and synaptic currents can each drive linear increases in MVN firing rates

A, The firing rate of an example YFP-16 neuron during 1 s steps of depolarizing somatic current injection of varying amplitudes (inset). Neuronal firing rates, averaged over the 1 s step, were linearly related to injected current. B, Synaptic stimulation for 1 s drives increases in firing rate in the same neuron shown in A. Somatic current injection was used to maintain a stable baseline firing rate of ~5 Hz. C, The postsynaptic firing rate in this neuron at the two synaptic stimulation rates shown (20 and 100 Hz). D, Linear input to firing rate relationship for the neuron shown in C. The slope is less than 1, indicating the linear synaptic summation of input currents over time. E, Summary of goodness of linear fits in response to stimuli that ranged from 20 to 150 Hz rates in the population of YFP-16 and GIN neurons. F, Summary of firing response gains across the same population. Of the 8 GIN and 10 YFP-16 neurons tested, only one fired action potentials with every presynaptic stimulus (gain = 1).